

Supporting information

Electrodeposition of thick palladium coatings from a palladium(II)-containing ionic liquid

Stijn Schaltin, Neil R. Brooks, Jeroen Sniekers, Luc Van Meervelt,
Koen Binnemans, Jan Fransaer

Synthesis

General

All chemicals were purchased from Acros Organics (Geel, Belgium) or IoLiTec (Heilbronn, Germany) and were of reagent grade and used without further purification. Palladium(II) acetate was used as a starting reagent for the synthesis of all palladium liquid metal salts. Since the direct reaction of the starting reagent with the ligand and the anion in acidic form gave no result, a different synthesis route was followed. A solution of the palladium(II) acetate and two equivalents of ligand were reacted with two equivalents of a protic ionic liquid. The anions of the protic ionic liquid become the anions of the liquid metal salt while the cations of the protic ionic liquid act as two ligands. The other two ligands of the liquid metal salt are from the free ligands that are also added to the solution. Acetic acid is formed during reaction and is removed on a rotary evaporator, together with the solvent.

Synthesis of [MeImH][Tf₂N]

A mixture of hydrogen bistriflimide (3.43 g, 12.2 mmol from an 80% aqueous solution) and a slight excess of *N*-methylimidazole (1.20 g, 14.6 mmol) formed a biphasic mixture at room temperature. The solution was stirred for 15 min. at room temperature, 15 min. at 50 °C and 15 min. at 80 °C until a homogeneous, clear liquid was obtained. This was dried overnight on a Schlenk line at 80 °C to remove the excess of *N*-methylimidazole and water. The product spontaneously crystallized after a few days to form white crystals. FTIR (ATR, ν/cm^{-1}): 3270, 3151, 1585, 1549, 1349, 1328, 1306, 1180 (CF₃), 1128 (SO₂), 1051 (SNS), 792, 766, 744 (CF₃), 606 (SO₂), 570 (CF₃), 513 (CF₃). Melting point: 44 °C.

Synthesis of [EtImH][Tf₂N]

A mixture of hydrogen bistriflimide (2.92 g, 10.4 mmol from an 80% aqueous solution) and a slight excess of *N*-ethylimidazole (1.20 g, 12.4 mmol) formed a biphasic mixture at room temperature. The solution was stirred for 15 min. at room temperature, 15 min. at 50 °C and 15 min. at 80 °C until a homogeneous, clear liquid was obtained. This was dried overnight on a Schlenk line at 80 °C to remove the excess of *N*-ethylimidazole and water. The resulting product was a clear liquid. FTIR (ATR, ν/cm^{-1}): 3105, 2980, 2939, 1508, 1464, 1446, 1353, 1326 (SO₂), 1286, 1224 (CF₃), 1227, 1198 (CF₃), 1141 (SO₂), 1061 (SNS), 1034, 957, 907, 815, 747 (CF₃), 737, 665, 623, 608 (SO₂), 572 (CF₃), 513 (CF₃).

Synthesis of [Pd(MeIm)₄][Tf₂N]₂

A solution of palladium(II) acetate (2.00 g, 8.91 mmol), *N*-methylimidazole (1.44 g, 17.82 mmol) and [MeImH][Tf₂N] (6.48 g, 17.82 mmol) in acetonitrile was stirred for 3 h at 80 °C. Excess solvent was removed on a rotary evaporator and the resulting yellow solid was dried on a high vacuum line. Yield: 8.61 g (97%). CHN found (calculated for C₂₀H₂₄N₁₀S₄O₈F₁₂Pd): C 24.39 (24.14)%, H 2.34 (2.43)%, N 13.95 (14.08)%. IR (ATR, ν/cm^{-1}): 3145 (CH), 1544, 1529, 1427, 1353, 1175 (CF₃), 1134 (SO₂), 1108, 1047 (SNS), 821, 739 (CF₃), 655, 614 (SO₂), 602, 568 (CF₃), 508. NMR: δ_{H} (300 MHz, CDCl₃): 7.99 (s), 7.07 (t), 6.84 (t), 3.70 (s); δ_{C} (75 MHz, CDCl₃): 138.92 (s), 128.61 (s), 121.71 (s), 119.82 (q), 34.87 (s). Melting point: 105 °C.

Crystal data for $C_{20}H_{24}F_{12}N_{10}O_8PdS_4$ ($M = 995.13 \text{ g mol}^{-1}$): monoclinic, space group $P2_1/c$ (no. 14), $a = 9.1556(2) \text{ \AA}$, $b = 10.8229(2) \text{ \AA}$, $c = 17.9774(3) \text{ \AA}$, $\beta = 99.330(2)^\circ$, $V = 1757.82(6) \text{ \AA}^3$, $Z = 2$, $T = 100(2) \text{ K}$, $\mu(\text{MoK}\alpha) = 0.888 \text{ mm}^{-1}$, $D_{\text{calc}} = 1.880 \text{ g cm}^{-3}$, 8254 reflections measured ($5.88^\circ < 2\Theta < 58.2^\circ$), 4114 unique ($R_{\text{int}} = 0.0174$, $R_{\text{sigma}} = 0.0287$) which were used in all calculations. The final R_1 was 0.0256 ($>2\sigma(I)$) and wR_2 was 0.0615 (all data).

Synthesis of $[Pd(\text{MeIm})_2(\text{EtIm})_2][\text{Tf}_2\text{N}]_2$

A solution of palladium(II) acetate (2.00 g, 8.91 mmol), *N*-ethylimidazole (1.71 g, 17.82 mmol) and $[\text{MeImH}][\text{Tf}_2\text{N}]$ (6.48 g, 17.82 mmol) in acetonitrile was stirred for 3 h at 80 °C. Excess of solvent was removed on a rotary evaporator and the resulting yellow solid was dried on a high vacuum line. Yield: 8.75 g (96%). CHN found (calculated for $C_{22}H_{28}F_{12}N_{10}O_8S_4Pd$): C 25.53 (25.82)%, H 2.92 (2.75)%, N 13.48 (13.69)%. IR (ATR, ν/cm^{-1}): 3144 (CH), 2988, 1528, 1349, 1335, 1179 (CF_3), 1138 (SO_2), 1107, 1050 (SNS), 833, 758, 740 (CF_3), 665, 655, 608, 568 (CF_3), 511, 408. NMR: δ_{H} (300 MHz, CDCl_3): 7.98 (s), 6.99 (t), 6.94 (t), 3.98 (q), 3.66 (s), 1.33 (t); δ_{C} (75 MHz, CDCl_3): 138.46 (s), 128.04 (s), 122.33 (s), 119.76 (q), 43.48 (s), 34.71 (s), 15.22 (s). Melting point: 45 °C.

Crystal data for $C_{22}H_{28}F_{12}N_{10}O_8PdS_4$ ($M = 1023.18 \text{ g mol}^{-1}$): monoclinic, space group $P2_1/c$ (no. 14), $a = 10.2427(8) \text{ \AA}$, $b = 11.3109(5) \text{ \AA}$, $c = 15.6582(9) \text{ \AA}$, $\beta = 90.056(6)^\circ$, $V = 1814.07(18) \text{ \AA}^3$, $Z = 2$, $T = 100(2) \text{ K}$, $\mu(\text{MoK}\alpha) = 0.864 \text{ mm}^{-1}$, $D_{\text{calc}} = 1.873 \text{ g cm}^{-3}$, 9615 reflections measured ($5.96^\circ < 2\Theta < 58.24^\circ$), 4200 unique ($R_{\text{int}} = 0.0169$, $R_{\text{sigma}} = 0.0259$) which were used in all calculations. The final R_1 was 0.0365 ($>2\sigma(I)$) and wR_2 was 0.0978 (all data).

Synthesis of $[Pd(\text{EtIm})_4][\text{Tf}_2\text{N}]_2$

A solution of palladium(II) acetate (2.00 g, 8.91 mmol), *N*-ethylimidazole (1.71 g, 17.82 mmol) and $[\text{EtImH}][\text{Tf}_2\text{N}]$ (6.72 g, 17.82 mmol) in acetonitrile was stirred for 3 h at 80 °C. Excess of solvent was removed on a rotary evaporator and the resulting yellow solid was dried on a high vacuum line. Yield: 9.09 g (97%). CHN found (calculated for $C_{24}H_{32}F_{12}N_{10}O_8PdS_4$): C 27.30 (27.42)%, H 3.47 (3.07)%, N 13.15 (13.32)%. IR (ATR, ν/cm^{-1}): 3145 (CH), 2985 (CH), 1536, 1527, 1450, 1350, 1336, 1241, 1181 (CF_3), 1140 (SO_2), 1103, 1052 (SNS), 968, 860, 844, 789, 741 (CF_3), 666, 655, 608, 568 (CF_3), 512, 409. NMR: δ_{H} (300 MHz, CDCl_3): 7.93 (s), 7.01 (t), 6.91 (t), 3.99 (q), 1.39 (t); δ_{C} (75 MHz, CDCl_3): 137.76 (s), 128.45 (s), 120.15 (s), 119.93 (q), 43.52 (s), 15.43 (s). Melting point: 76 °C.

Crystal data for $C_{24}H_{32}F_{12}N_{10}O_8PdS_4$ ($M = 1051.24 \text{ g mol}^{-1}$): triclinic, space group $P-1$ (no. 2), $a = 8.8459(5) \text{ \AA}$, $b = 9.1693(6) \text{ \AA}$, $c = 14.3228(9) \text{ \AA}$, $\alpha = 92.776(5)^\circ$, $\beta = 106.337(5)^\circ$, $\gamma = 113.370(6)^\circ$, $V = 1006.34(11) \text{ \AA}^3$, $Z = 1$, $T = 100(2) \text{ K}$, $\mu(\text{MoK}\alpha) = 0.781 \text{ mm}^{-1}$, $D_{\text{calc}} = 1.735 \text{ g cm}^{-3}$, 8744 reflections measured ($5.84^\circ < 2\Theta < 58.14^\circ$), 4580 unique ($R_{\text{int}} = 0.0171$, $R_{\text{sigma}} = 0.0261$) which were used in all calculations. The final R_1 was 0.0240 ($>2\sigma(I)$) and wR_2 was 0.0581 (all data).

Characterization

TGA studies were performed on a TA instruments Q600 thermogravimeter. The temperature was scanned from room temperature up to 800 °C at 5 °C min^{-1} in an argon atmosphere (Fig. 1). The infrared spectra were recorded at a resolution of 4 cm^{-1} , using an attenuated total reflectance (ATR) technique on a Bruker Vertex 70 FTIR spectrometer, with a Platinum ATR extension (Fig. 2). Assignment of the peaks was based on literature data.^{1,2} Melting points were determined with a Mettler-Toledo 822 DSC instrument using a heating rate of 10 °C min^{-1} in a helium atmosphere. FTIR spectra were recorded with a Bruker Vertex 70 FTIR spectrometer, equipped with a Platinum ATR accessory. ^1H and ^{13}C NMR measurements were done with a Bruker Avance 300 MHz spectrometer. Elemental analyses (C, H, N) were performed by using a CE Instruments EA-1110 elemental analyzer. Dynamic viscosities μ (Table 1) have been

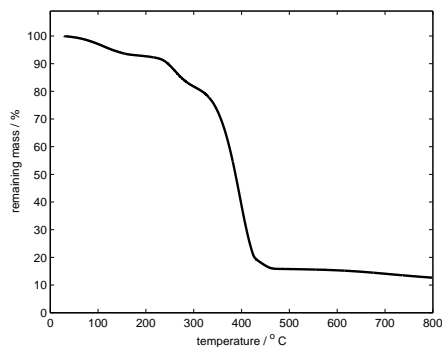


Figure 1: TGA trace of $[\text{Pd}(\text{MeIm})_2(\text{EtIm})_2][\text{Tf}_2\text{N}]_2$.

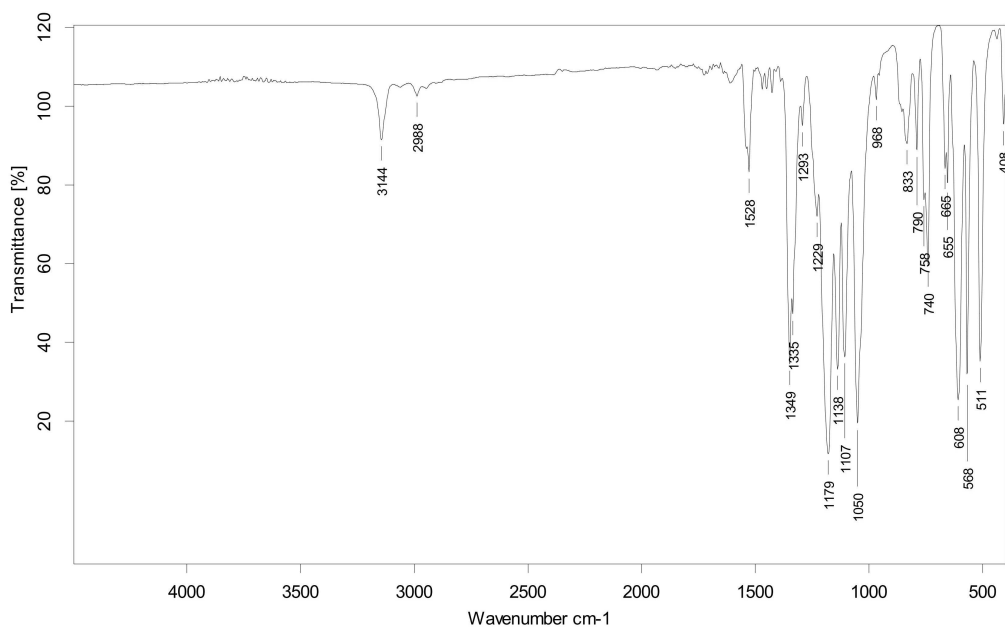


Figure 2: IR spectrum of $[\text{Pd}(\text{MeIm})_2(\text{EtIm})_2][\text{Tf}_2\text{N}]_2$.

measured with a Brookfield cone plate viscometer (LVDV-II+ Programmable Viscometer) with a cone spindle CPE-40. The ionic liquid was kept under dry nitrogen atmosphere during the measurement and the temperature of the sample was controlled by a circulating water bath.

Table 1: Dynamic viscosity of $[\text{Pd}(\text{MeIm})_2(\text{EtIm})_2][\text{Tf}_2\text{N}]_2$.

T / °C	μ / mPa s
60	153
70	97
80	63

Crystallography

Crystals of $[\text{Pd}(\text{MeIm})_4][\text{Tf}_2\text{N}]_2$, $[\text{Pd}(\text{EtIm})_4][\text{Tf}_2\text{N}]_2$ and $[\text{Pd}(\text{MeIm})_2(\text{EtIm})_2][\text{Tf}_2\text{N}]_2$ suitable for single crystal X-ray diffraction were mounted into the cold stream of an Oxford Cryostreams cryocooler at 100(2) K on a nylon loop attached to a copper pin and placed on an Agilent SuperNova diffractometer using Mo K α radiation ($\lambda = 0.71073 \text{ \AA}$). The absorption corrections were applied using CrysAlisPro.³ All structures were solved using direct methods and refined

by the full-matrix least-squares procedure in SHELXL.⁴ All hydrogen atoms were placed in calculated positions and refined using a riding model. The program OLEX2 was also used in refinement and making pictures.⁵ CCDC 1003259-1003261 contains the supplementary crystallographic data for this paper. In all structures the $[\text{Pd}(\text{AlkIm})_4]^{2+}$ cations had the expected square-planar geometry with similar Pd–N bond distances (Table 2). In the structure of

Table 2: Pd–N bond distances and N–Pd–N bond angles in the structures of $[\text{Pd}(\text{MeIm})_4][\text{Tf}_2\text{N}]_2$, $[\text{Pd}(\text{EtIm})_4][\text{Tf}_2\text{N}]_2$ and $[\text{Pd}(\text{MeIm})_2(\text{EtIm})_2][\text{Tf}_2\text{N}]_2$.

	Pd–N / Å	N–Pd–N / °
$[\text{Pd}(\text{MeIm})_4][\text{Tf}_2\text{N}]_2$	2.0131(15)	88.95(6)
	2.0151(16)	180
$[\text{Pd}(\text{EtIm})_4][\text{Tf}_2\text{N}]_2$	2.0208(13)	89.46(5)
	2.0165(13)	180
$[\text{Pd}(\text{MeIm})_2(\text{EtIm})_2][\text{Tf}_2\text{N}]_2$	2.012(2)	89.69(10)
	2.012(2)	180

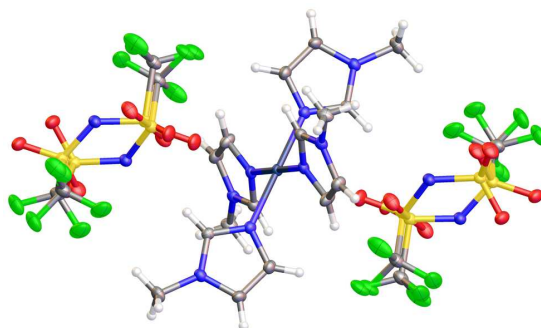


Figure 3: View of the crystal structure of $[\text{Pd}(\text{MeIm})_4][\text{Tf}_2\text{N}]_2$ showing the cation and the disorder in the anion (displacement ellipsoids shown at the 50% probability level).

$[\text{Pd}(\text{MeIm})_4][\text{Tf}_2\text{N}]_2$ (Fig. 3), the $[\text{Pd}(\text{MeIm})_4]^{2+}$ cation was found on a site with inversion symmetry so only half the cation is located in the asymmetric unit. The $[\text{Tf}_2\text{N}]^-$ anions were on a general position but found to be disordered so they were modeled as two disordered components (Fig. 3) with a refined population factor showing the major disorder component comprising 94.6(1)% of the total. The bond lengths and thermal parameters for the minor disorder component were restrained to be the same as those of the major component. The packing, viewed along the crystallographic a axis is shown in Fig. 4. In the structure of $[\text{Pd}(\text{EtIm})_4][\text{Tf}_2\text{N}]_2$ (Fig. 5) the $[\text{Pd}(\text{EtIm})_4]^{2+}$ cation was found on a site with inversion symmetry so only half the cation is located in the asymmetric unit. In addition, there were two $[\text{Tf}_2\text{N}]^-$ anions also on inversion centres and as $[\text{Tf}_2\text{N}]^-$ does not possess inversion symmetry these are disordered over two positions with a 50:50 ratio (Fig. 5). The packing, viewed along the crystallographic b axis is shown in Fig. 6. In the structure of $[\text{Pd}(\text{MeIm})_2(\text{EtIm})_2][\text{Tf}_2\text{N}]_2$ (Fig. 7) the $[\text{Pd}(\text{MeIm})_2(\text{EtIm})_2]^{2+}$ cation was found on a site with inversion symmetry so only half the cation is located in the asymmetric unit. This site symmetry causes disorder of the methyl and ethyl groups on the imidazole ligands (Fig. 7). There are two possible isomers of the $[\text{Pd}(\text{MeIm})_2(\text{EtIm})_2]^{2+}$ cation: *cis* and *trans*. Whilst the symmetry of the *cis* isomer is not compatible with the inversion symmetry of the crystallographic site, the *trans* isomer does have inversion symmetry. This may lead to the conclusion that the $[\text{Pd}(\text{MeIm})_2(\text{EtIm})_2]^{2+}$ cation in this structure is the *cis* isomer but disordered, however, it is possible that the *trans* isomer could occupy two positions related by a 90° rotation in the plane of the molecule and the resulting structure would look disordered the same as seen, so it is not possible to distinguish between *cis* and *trans*. In the refinement of the structure the position of the methyl group and methylene unit of the ethyl group were constrained to be at the same position. The thermal parameters of the methyl and ethyl groups were a little bit larger than the imidazole rings due to the disorder. The packing, viewed along the crystallographic b axis is shown in Figs. 8 and

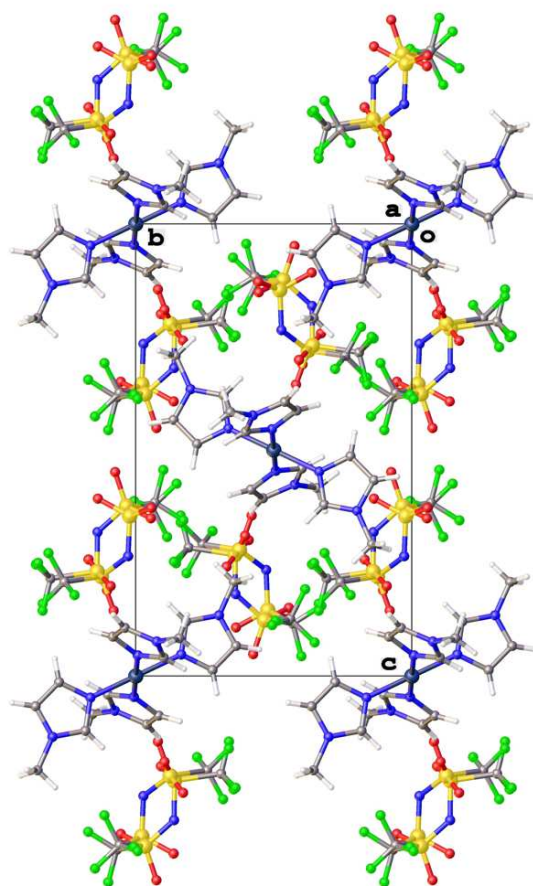


Figure 4: View of the packing in the crystal structure of $[\text{Pd}(\text{MeIm})_4][\text{Tf}_2\text{N}]_2$.

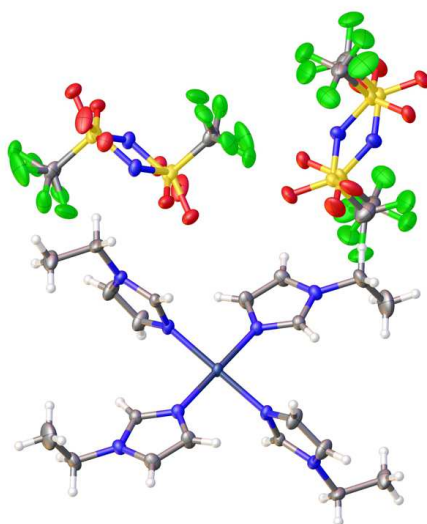


Figure 5: View of the crystal structure of $[\text{Pd}(\text{EtIm})_4][\text{Tf}_2\text{N}]_2$ showing the cation and the disorder in the anions (displacement ellipsoids shown at the 50% probability level).

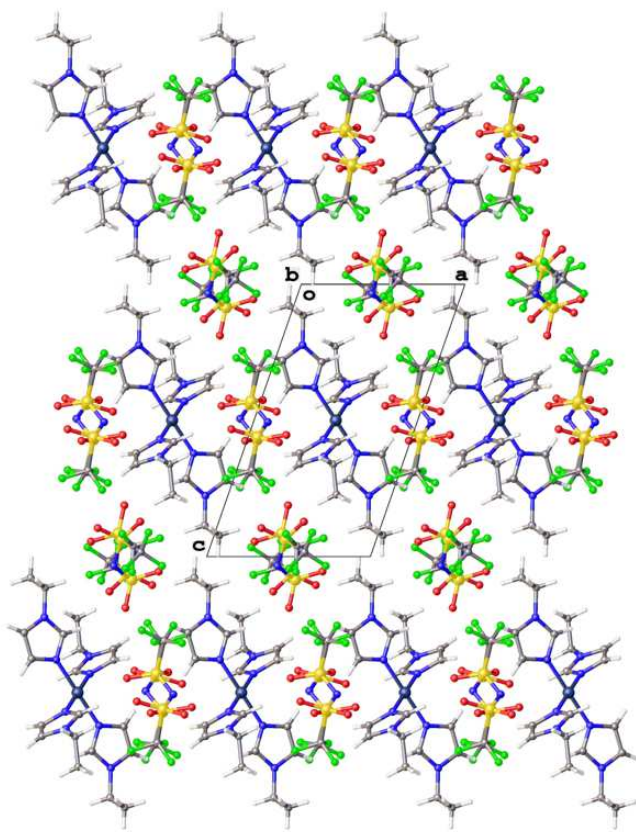


Figure 6: View of the packing in the crystal structure of $[\text{Pd}(\text{EtIm})_4][\text{Tf}_2\text{N}]_2$.

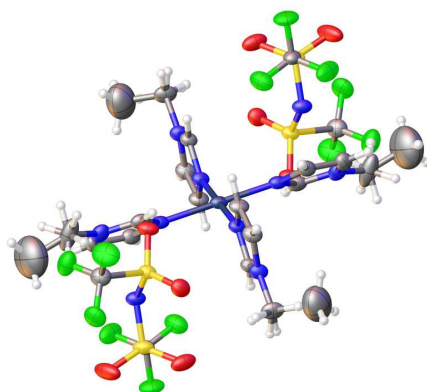


Figure 7: View of the crystal structure of $[\text{Pd}(\text{MeIm})_2(\text{EtIm})_2][\text{Tf}_2\text{N}]_2$ showing the disorder of the cation and the anions (displacement ellipsoids shown at the 50% probability level).

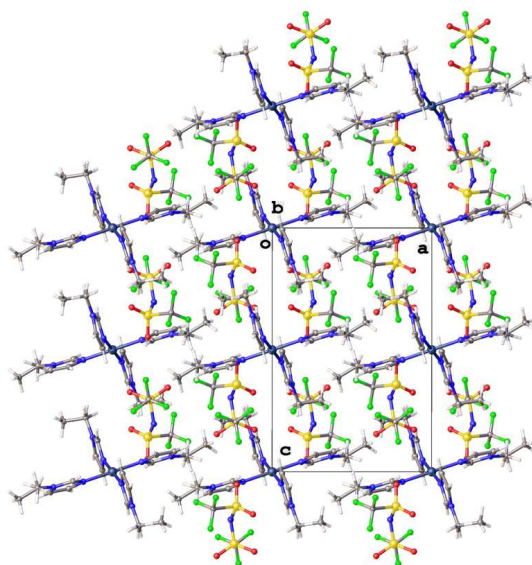


Figure 8: View of the packing in the crystal structure of $[\text{Pd}(\text{MeIm})_2(\text{EtIm})_2][\text{Tf}_2\text{N}]_2$.

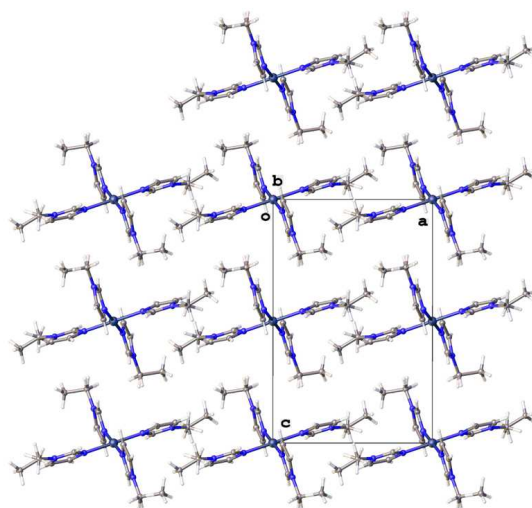


Figure 9: View of the packing in the crystal structure of $[\text{Pd}(\text{MeIm})_2(\text{EtIm})_2][\text{Tf}_2\text{N}]_2$ without $[\text{Tf}_2\text{N}]^-$ anions for clarity.

9 with and without the $[\text{Tf}_2\text{N}]^-$ anions, respectively. Although the unit cell has three angles of 90° , the crystal structure has monoclinic symmetry and shows no sign of twinning.

Electrochemistry

Gold-covered silicon wafers were used as working electrodes (Si, 500 nm SiO_2 , 10 nm Ti, 100 nm Au). Before use, the substrates were cleaned by rinsing with acetone and dried. After the deposition of a silver layer, the deposit was rinsed with water and ethanol, and dried. The electrolyte was contained in a platinum crucible, and it was not stirred during the experiments. The temperature was held at 70°C for all electrochemical experiments, unless mentioned otherwise. These experiments were done using a Potentiostat/Galvanostat EG&G 273 controlled by a computer with Corrware software. All potential values in this paper are relative to a palladium wire directly immersed in solution (pseudo-reference electrode). A palladium coil was used as counter electrode. Cyclic voltammograms were measured at a scan rate of 50 mV s^{-1} . Deposits were made potentiostatically at -1.0 or -1.5 V . All electrochemical experiments were performed in an argon-filled glove box (with O_2 and H_2O concentrations below 1 ppm). Quartz crystal Microbalance (QCM) experiments were conducted with a Maxtex RQCM apparatus. The morphology and elemental composition of the deposits were determined by scanning electron microscopy (SEM) and energy-dispersive X-ray analysis (EDX) (Philips XL 30 FEG).

The influence of the scan rate ν (varied as $\nu = 5, 10, 20, 50, 100, 200\text{ mV s}^{-1}$) on the cyclic voltammogram is presented in Fig. 10. The height of the anodic peak is strongly dependent on ν and almost disappears for small values of ν . This means that the anodic dissolution of deposited palladium does not occur, proving the irreversibility of the deposition reaction.

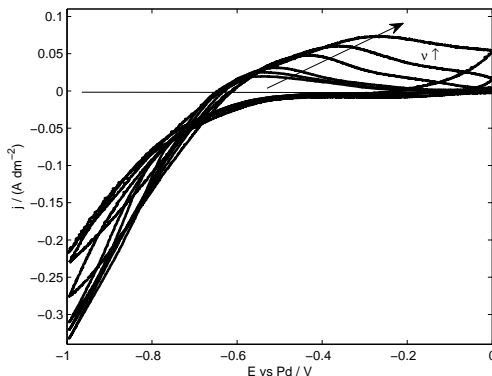


Figure 10: Cyclic voltammograms of $[\text{Pd}(\text{MeIm})_2(\text{EtIm})_2][\text{Tf}_2\text{N}]_2$ with different scan rates ν ($\nu = 5, 10, 20, 50, 100, 200\text{ mV s}^{-1}$).

The irreversibility is even more clear from potentiostatic experiments. Fig. 11 shows the QCM results for $[\text{Pd}(\text{MeIm})_2(\text{EtIm})_2][\text{Tf}_2\text{N}]_2$ during which the potential is jumped from -1.0 V where deposition takes place to three anodic potentials of 0.0 V , $+0.5\text{ V}$ and $+1.0\text{ V}$. This potential function is given in Fig. 11(a). The measured current i and frequency shift Δf are shown in Figs. 11 (b) and (c). The Δf signal goes down when the potential is -1.0 V meaning that material is deposited, but it does not go up when anodic potentials are applied, irrespective whether this anodic potential is 0.0 V , $+0.5\text{ V}$ or $+1.0\text{ V}$. This observation shows the irreversibility of palladium deposition from $[\text{Pd}(\text{MeIm})_2(\text{EtIm})_2][\text{Tf}_2\text{N}]_2$. The solid line in Fig. 11(d) represents the experimental mass, based on Δf while the dashed line is a theoretical mass based on Faraday's law of electrochemistry and assuming that all the current is used for the reduction of $\text{Pd}(\text{II})$ to metallic palladium. The perfect correspondence between theory and experiment proves that the deposition of palladium from $[\text{Pd}(\text{MeIm})_2(\text{EtIm})_2][\text{Tf}_2\text{N}]_2$ occurs with a current efficiency of 100%.

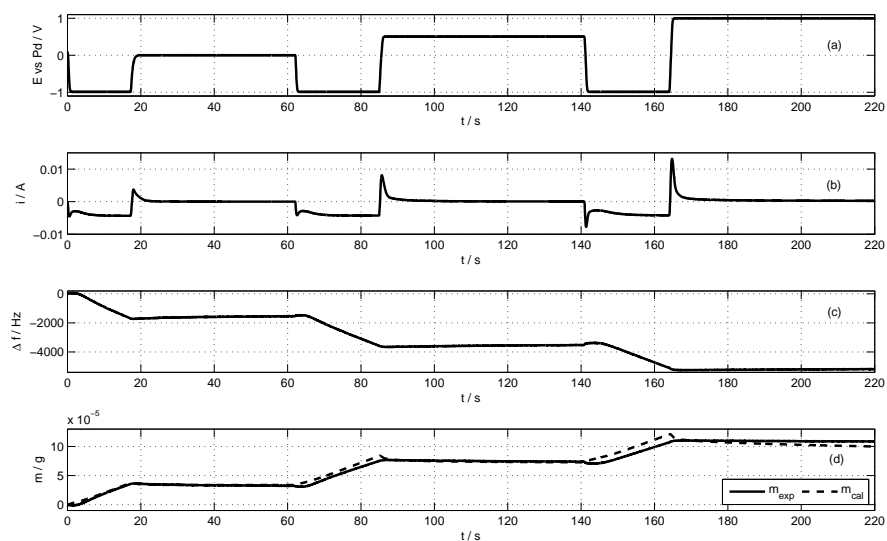


Figure 11: QCM-data of $[\text{Pd}(\text{MeIm})_2(\text{EtIm})_2][\text{Tf}_2\text{N}]_2$ showing (a) the applied potential function E , (b) the measured current i , (c) the frequency shift Δf and (d) the measured and theoretically calculated masses m .

References

- [1] I. Rey, P. Johansson, J. Lindgren, J. C. Lassègues, J. Grondin and L. Servant, *J. Phys. Chem. A*, 1998, **102**, 3249.
- [2] J. B. Hodgson, G. C. Percy and D. A. Thronton, *J. Mol. Struct.*, 1980, **66**, 81.
- [3] *CrysAlisPro*, Agilent Technologies, Yarnton, UK, 2013.
- [4] G. M. Sheldrick, *Acta Cryst.*, 2008, **A64**, 112.
- [5] A. V. Dolomanov, L. J. Bourhis, R. J. Gildea, J. A. K. Howard and H. Puschmann, *J. Appl. Crystallogr.*, 2009, **42**, 339.